High resolution Compton scattering study of Be

K. Hämäläinen and S. Manninen
Department of Physics, P.O. Box 9, FIN-00014 University of Helsinki, Finland

C.-C. Kao, W. Caliebe, and J. B. Hastings
National Synchrotron Light Soource, Brookhaven National Laboratory, Upton, New York 11973

A. Bansil and S. Kaprzyk*
Department of Physics, Northeastern University, Boston, Massachusetts 02115

P. M. Platzman
AT&T Bell Laboratories, 600 Mountain Avenue, Murray Hill, New Jersey 07974
(Received 15 January 1996)

We have carried out high-resolution Compton scattering measurements from two single crystals of Be ([00.1] and [11.0]), together with highly accurate all-electron first-principles computations of the profiles within the band theory framework. The Compton data were collected using a newly constructed crystal spectrometer at a record momentum resolution varying between 0.023 and 0.032 a.u. (full width at half maximum) with 8 keV x rays from a synchrotron source. Although the overall shapes of the measured and computed spectra are in good accord, the fine structure in the data shows significant discrepancies with respect to the local density approximation based theoretical predictions. In particular, several features in the observed spectra are substantially broader than the computations, indicating the importance of electron correlations and other effects in analyzing momentum densities and Compton profiles from solids. [S0163-1829(96)02132-7]

I. INTRODUCTION

Inelastic scattering of x rays at large momentum transfers, usually referred to as Compton scattering, constitutes a powerful spectroscopy of the ground state electronic structure of materials. In the case of metals, the Compton technique offers unique possibilities as a direct probe of Fermi surface (FS) signatures and correlation effects in the electron momentum density. However, progress in this regard has been limited by the fact that the necessary experimental resolution has been lacking. Since Fermi momenta are typically of order 1 a.u., a high momentum resolution — of < 0.1 a.u. or better — is essential for delineating FS features. The recent advent of synchrotron sources has made it possible to construct spectrometers[1–3] capable of resolutions of this order, throwing open new opportunities for the application of the Compton scattering technique.

We want to emphasize that the Compton scattering spectroscopy should be viewed as being complementary to other relevant Fermi surface spectroscopies such as de Haas–van Alphen (dHvA), two-dimensional angular correlation of annihilation radiation (2D-ACAR), and angle-resolved photoemission, since each technique possesses its own relative advantages and disadvantages. Compton spectroscopy does not suffer from the requirement of extremely pure samples (dHvA, 2D-ACAR), low temperature (dHvA), positron electron correlation (2D-ACAR), or surface sensitivity (photoemission). On the other hand, in the Compton scattering all the electrons are contributing to the scattering cross section and the profile is related to one-dimensional projection of the momentum density.

Most of the existing Compton spectrometers are based on the measurement of the energy spectrum of the scattered photons via various types of position sensitive detectors. In contrast, our approach is to vary the energy of the *incident* beam, holding the energy of the scattered beam fixed, allowing us to use an extreme backscattering geometry for the analyzer crystal minimizing the source size effects. Additionally, such a setup possesses the advantage that we can collect data in any specific momentum range and thus focus selectively on interesting spectral details. The final Compton profile is studied on a momentum scale p_z which is uniquely determined for a given scattering angle by the incident and scattered photon energies. Therefore it does not make any fundamental difference which one of these energies is varied in order to obtain the Compton profile. Recently, a spectrometer suitable for Compton scattering studies has been constructed along these lines at the National Synchrotron Light Source (NSLS).[4,5] This spectrometer is capable of delivering a momentum resolution of about 0.02 a.u., approximately five times better than the best earlier experiments, although at the $\sim$8 keV beam energy available at the NSLS, one will be limited to investigations of valence electrons in relatively low Z materials. A similar spectrometer is also under commissioning at the European Synchrotron Radiation Facility (ESRF), Grenoble. We note that the idea of scanning the energy of the incident rather than the scattered photons was first employed by Schülke and Nagasawa,[6] although their main interest was the analysis of collective excitations (plasmons) and the dynamic structure factor in the low and the intermediate momentum transfer regime.

This article reports results of experiments carried out at NSLS to demonstrate the high resolution of the new Compton spectrometer. Data from two Be single crystals with surface normals along the [00.1] and [11.0] directions are pre-

sented, and analyzed with the help of corresponding highly accurate all-electron computations within the band theory framework. Be is a good test case for exploring solid state effects because as many as half of its electrons are involved in bonding; in fact, the Be Compton spectra are well known to exhibit one of the largest anisotropies among the elemental solids. In addition, x-ray diffraction, neutron diffraction, and the earlier Compton scattering data from Be have shown that the contribution of the 1*s* electrons to the charge density is anomalous.[7–9]

Previous momentum density experiments on Be have involved the use of conventional x-ray sources,[10] synchrotron radiation,[11] γ rays,[12] as well as positron annihilation.[13] On the theoretical side, computations of the Compton profiles (CP's) based on pseudopotentials[11] and the self-consistent-field linear combination of atomic orbitals (SCF-LCAO) method[14] have been reported. We emphasize, however, that much of this earlier theoretical as well as experimental work on Be does not possess sufficient resolution to permit a serious discussion of fermiology-related issues which clearly require an analysis of fine structural details in the CP's.

An outline of this article is as follows. The introductory remarks in Sec. I are followed by experimental and theoretical details in Secs. II and III, respectively. Section IV presents and discusses the main results concerning the CP's. Section V gives a brief summary with some concluding comments.

II. EXPERIMENT

The experiments were carried out on the high resolution inelastic scattering beamline X21 (Ref. 5) at the National Synchrotron Light Source (U.S.A.). The radiation from the multipole wiggler source was monochromatized and focused horizontally using a cylindrically bent triangular Si [220] crystal with an asymmetry angle of 19°, operated in the Rowland circle geometry; no vertical focusing element was used. The energy bandwidth of the incident beam was about 0.7 eV at 8 keV, the resolution being limited by the source size (finite length of the insertion device). The beam possessed a focal size of 0.2 mm horizontal $\times$ 10 mm vertical with a monochromatic flux at the sample of about 2×10^{11} photons/s.

Since the simple relationship of the scattering cross section to the ground state momentum profile is only true at large momentum transfer[15,16] the experiment was carried out at a scattering angle of 160°. This is the maximum angle permitted by the physical position and size of the vacuum chamber. The analyzer was based on a spherically bent Si [444] crystal operated in the Rowland circle geometry as close as possible to backscattering. The analyzer possessed a radius of 1 m (realized by gluing the crystal to a spherical glass mold.[17]) A circular analyzer crystal area with a diameter of 67 mm was used in these measurements. The contribution of the analyzer to the total energy resolution of 0.8 eV was about 0.3 eV and limited by the source size (beam size at the sample) and imperfections in the bend. Various elements of the spectrometer (sample, analyzer crystal, and detector) were placed in a horizontal scattering plane.

The photons from the analyzer were measured with a standard NaI detector. The background level, obtained by misplacing the detector from the focus, was less than 0.1 counts/s. The incident photon flux changes due to electron beam decay; further, the changes are energy dependent as a result of the spectral bandwidth of the insertion device and the monochromator reflection properties. Therefore the incident flux was monitored by measuring current from an air-filled ionization chamber, corrected for air absorption ($\propto E^{-3}$) and ion production ($\propto E$) efficiency. The validity of this procedure was further confirmed by comparing the ion chamber results with the scattering cross section obtained from a thin amorphous foil with a NaI detector over the full scanning range. In this respect, scanning the incident instead of the scattered photon energy possesses a clear advantage because the overall efficiency of the system can be measured and the data corrected reliably as a function of energy. With position sensitive detectors and dispersive optics, on the other hand, the efficiency correction is always more complicated.

One potentially serious drawback of scanning the incident rather than the scattered photon energy should be noted. A ''glitch'' in the measured CP appears whenever the scattering vector satisfies the diffraction condition for the sum of two lattice vectors because the resulting multiple scattering Bragg peak causes the change of the effective flux at the sample. We have taken special care to avoid such glitches in the present measurements. For this purpose, an ionization chamber was placed behind the sample and the transmission spectra were recorded simultaneously with the incident energy scan. The orientation of the sample was then tweaked slightly in a direction perpendicular to the scattering plane to search for an optimal position which avoids the glitches. This procedure should be successful more generally because even if all the glitches turn out to be unavoidable, the locations where they occur can be identified.

The samples were single crystals of Be. Two different orientations with surface normals along [00.1] and [11.0] were used. The [00.1] crystal was 2 mm thick in the shape of a rectangle 15 mm (width) $\times$ 10 mm (height). The [11.0] crystal was 2.9 mm thick in the shape of a cylinder of 20 mm diameter. The crystal thickness was chosen to be smaller than the absorption length for Be at these energies ($1/\mu\approx5$ mm) so that the multiple scattering effects in the sample as well as the effective source size for the analyzer were reduced. In order to avoid sample degradation due to oxidation, and also to reduce background associated with air scattering, the crystals were retained in an evacuated can with thin kapton windows during the measurements. The orientation of each sample was checked carefully after mounting in the sample stage by indexing some Bragg reflections using a phosphoric screen. In actual measurements the sample was turned to be in a symmetric reflection geometry ($\theta_{\rm in}=\theta_{\rm out}=80°$). Note that the scattering vector lies along the surface normal only at the elastic line. Over the full scanning range (430 eV), the scattering vector deviates by about half a degree from the surface normal. However, this is negligible compared, for example, with the angular resolution (more than 3°) associated with the finite size of the analyzer crystal.

In typical Compton experiments where photons of energy ω_1 and momentum $\mathbf{q}_1$ are scattered into photons of energy ω_2 and momentum of $\mathbf{q}_2$ ($\hbar=1$) the energy shift $\omega=\omega_1-\omega_2$ is given roughly by $\omega=q^2/2m+\mathbf{q}\cdot\mathbf{p}/m$ where

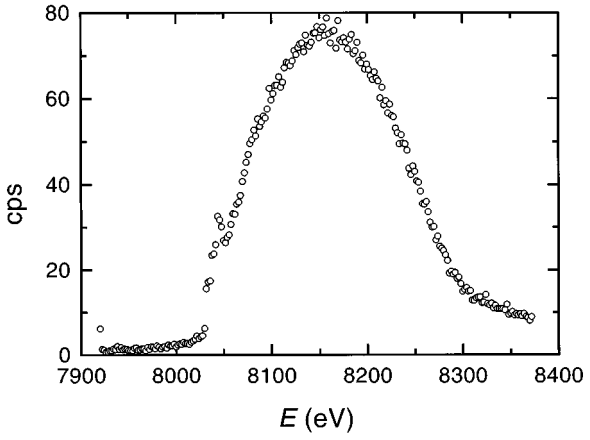

FIG. 1. Energy spectrum (raw data) from a polycrystalline Be sample having thickness of 250 μm. The elastic line is at 7920 eV. In the actual measurement from single crystal samples only data on the high energy side were collected.

$\mathbf{q}=\mathbf{q}_2-\mathbf{q}_1$ and $\mathbf{p}$ is the value of the electron's momentum in its ground state. In our case $q\simeq 2q_1\simeq 4p_F$ (p_F is the Fermi momentum of Be) and $q^2/2m\simeq 140$ eV. A typical energy spectrum is shown in Fig. 1. The spectra were obtained by scanning the incident photon energy for a fixed scattered photon energy (7920 eV) at the analyzing crystal Bragg angle of 86.9°. The incident energies were scanned from 8160 eV, to 8347 eV, which corresponds to the momentum range of -0.05 a.u. to 1.51 a.u. on the high energy loss side of the CP. The choice of the high energy loss side of the profile allows us to avoid the fine structure related to the Be K edge at $\omega = 112$ eV ($\simeq -1.13$ a.u.). Of course there is still a slowly varying $1s$ contribution present which gives a rather uniform background. However, in the difference profile between two different crystal orientations this contribution cancels out.

The spectra were collected with a step size of 0.5 eV (0.004 a.u.), the measurement time per point being 10 s. The count rate at the Compton peak was about 500 counts/s. For each crystal direction eight separate spectra were collected, yielding a total of 4×10^4 counts at the peak, and the associated statistical accuracy of 0.5%. At high momenta where the count rates were lower, the statistical accuracy was 1.1%. The total number of counts in the profile between 0 and 1.5 a.u. was about 10^7. Between separate scans the position of the elastic line was checked for possible energy drifts, but changes observed were less than 0.1 eV in all cases. In order to examine the possible presence of glitches and drifts as well as the validity of our normalization procedure, the eight normalized spectra for each orientation were compared to each other and found to be identical within the experimental statistics.

The summed spectrum for each crystal orientation was corrected for sample, air, and kapton window absorption which varied only by a few percent over the full scan range. The spectrum was then transformed to the momentum (p_z) scale using a standard relativistic formula.[18] No background subtraction was performed since, as already noted above, the background level in our experiment was insignificantly low. The fact that, at this stage, after all the corrections, the areas under the profiles for two independent crystals used were essentially the same, gives further confidence in our data handling procedures. Finally, the experimental spectra were renormalized so that the total area between 0 and 1.5 a.u. equals that under the corresponding theoretical profiles (1.59 electrons).

The multiple scattering events for our measurement were computed using a Monte Carlo simulation; for the two samples used in the experiment, this contribution is estimated to be about 7% and 9% (integrated over the full profile).[19,20] We expect these estimates to be overestimates since the simulation does not properly take into account the fact that the analyzer crystal effectively detects photons scattered only into a very narrow solid angle from a small irradiated volume. An effort to better model our experimental situation by modifying the existing multiple scattering codes is in progress.[19] For present purposes, the important point, however, is that the multiple scattering events give a rather smooth, slowly varying background to the single scattering profile. Therefore their inclusion has little effect on the anisotropies and the derivatives of the Compton profiles which are our main concern here. For these reasons, we have chosen not to correct the final Compton profiles given in this article for multiple scattering effects.

III. THEORY

The present computations are based on the all-electron charge self-consistent Korringa-Kohn-Rostoker (KKR) methodology.[21] The crystal potential is assumed to possess a nonoverlapping muffin-tin form, i.e., the potential is spherically symmetric within the muffin tins and constant (zero) outside. The exchange-correlation effects are incorporated within the von Barth–Hedin[22] local density approximation. As a prelude to the CP calculations, the band structure problem was solved to a high degree of self-consistency (energy bands, Fermi energy, and crystal potential converged to about 1 meV) for the hcp Be lattice ($a=4.3289$ a.u., $c=6.7675$ a.u.). Using the converged potential, the electronic wave functions were then obtained over 1800 *ab initio* $\mathbf{k}$ points in the irreducible 1/24th of the Brillouin zone (BZ). This basic data set permits an efficient evaluation of the electron momentum density $n(\mathbf{p})$ over a $24\times 1800\times 183$ $\mathbf{p}$-point mesh extending to about 5.0 a.u.; here each $\mathbf{k}$ point is translated via reciprocal lattice vectors to obtain $n(\mathbf{p})$ at 183 $\mathbf{p}$ points; the factor of 24 takes the symmetry of the lattice into account.

The CP along any direction may be computed by integrating $n(\mathbf{p})$ over a series of planes corresponding to different momentum transfers p_z along the surface normal. Care is necessary in carrying out these two-dimensional integrals since $n(\mathbf{p})$ varies rather slowly with momentum and possesses sharp structures arising from FS crossings. For this purpose, we have developed highly vectorized computer codes applicable to general lattices using the tetrahedral method of Lehmann and Taut.[23] Results for [00.1] and [11.0] CP's of Be have been obtained on a momentum mesh varying from 0.01 a.u. to 0.05 a.u., and are accurate to a few parts in 10^3. The total number of valence electrons is reproduced correctly to one part in 10^3 by the theoretical CP's over the range 0–5 a.u. The Lam-Platzman correction[24] to the CP's is

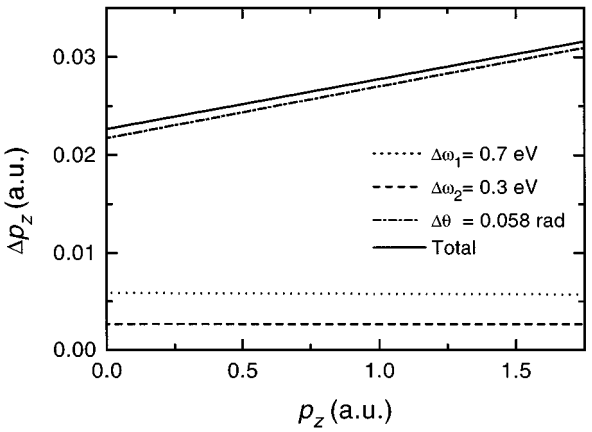

FIG. 2. Different contributions to the total momentum resolution for the parameters appropriate to this experiment. $\Delta\omega_1$ and $\Delta\omega_2$ refer to the effects of energy resolution of the incident and scattered beams. The total resolution is seen to be dominated by the uncertainty $\Delta\theta$ in the scattering angle due to the finite analyzer crystal size.

included based on the occupation number density for the uniform electron gas. Finally, we note that the overall shape and anisotropy of our CP's is consistent with the earlier theoretical CP's of Refs. 11 and 14.

IV. RESULTS AND DISCUSSION

We discuss the momentum resolution of our setup first with reference to Fig. 2. As can be seen from the figure the resolution varies slightly within our scanning range and is about 0.028 a.u. at the Be Fermi break. The total resolution was estimated by adding quadratically the partial contributions resulting from energy resolutions $\Delta\omega_1$ and $\Delta\omega_2$ of the incident and scattered photons, respectively, and the uncertainty $\Delta\theta$ in the scattering angle due to the finite size of the crystal analyzer. In this connection, the partial derivatives $\partial p_z/\partial\omega_1$, $\partial p_z/\partial\omega_2$, and $\partial p_z/\partial\theta$ were evaluated via exact analytical formulas. For our experiment, approximate formulas often used in the literature (see, e.g., Ref. 25) are not applicable, and yield, in particular, the contribution from $\Delta\theta$ which is too small roughly by a factor of 2 (see Appendix). Note that for experiments using dispersive optics with position sensitive detectors, the momentum resolution is dominated by the energy resolution. In contrast, with low energies and a relatively large size of the analyzer crystal, the momentum resolution in our case is dominated by the angular resolution (see Fig. 2) and could be improved significantly by slitting down the analyzer crystal opening at the expense of the count rate. Although we have chosen a rather large analyzer solid angle to achieve better statistics, a mosaic analyzer crystal with a relatively poor energy resolution (say $\sim$2 eV) would significantly increase detection efficiency with little degradation of the overall momentum resolution.

Before discussing the CP's, it will be helpful to recall that the FS of Be (Refs. 10 and 26) is well known to consist of two sheets, namely, the holelike ''coronet,'' and the electronlike ''cigars'' (see Figs. 10–12 of Ref. 26 for illustrations of these FS sheets). With two atoms per hcp unit cell

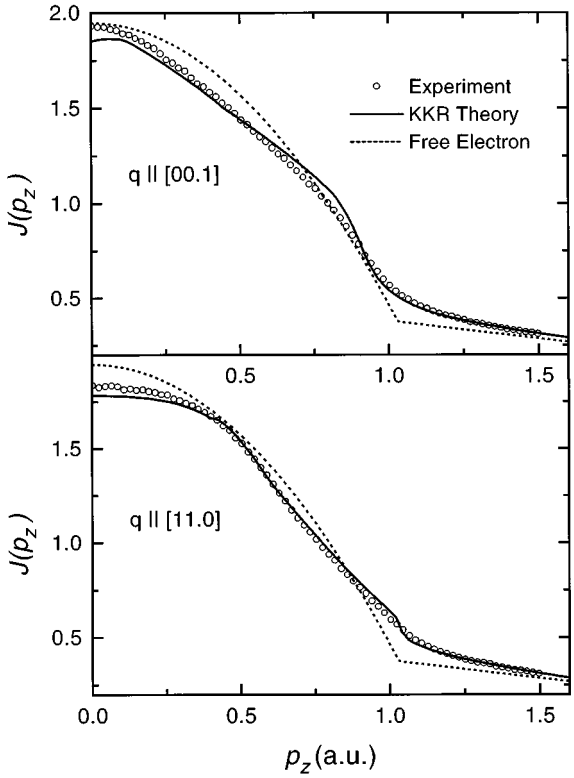

FIG. 3. Experimental Compton profiles along the [00.1] and [11.0] directions are compared with the corresponding resolution broadened theoretical profiles (solid lines). An appropriately normalized free-electron parabola combined with the theoretical core profile is also shown (dashed). The statistical error in the experimental data is smaller than the size of the plotting symbol.

and two valence electrons per atom, Be contains four electrons per unit cell which can in principle be accommodated in two full bands. In the actual system, however, the third band is partially occupied, yielding the cigars, leaving an equal number of holes in the second band corresponding to the coronet.

The directional CP's are presented in Fig. 3.[27] The overall shape of the [00.1] as well as the [11.0] profile is in reasonable accord between theory and experiment. The profiles are seen to differ substantially from the free-electron parabola, indicating that solid state effects are quite strong in Be. In this connection, Fig. 4, which shows the three-dimensional (3D) electron momentum density $\rho(\mathbf{p})$ along the principal symmetry directions, is illustrative. In the [00.1] direction, as a band gap opens up, $\rho(\mathbf{p})$ varies smoothly through the free-electron radius, and remains quite high up to the boundary $2\pi/c$ of the second BZ after which it decays rapidly. In contrast, $\rho(\mathbf{p})$ is more or less free-electron-like in the [11.0] and [10.0] directions. An examination of the computed $\rho(\mathbf{p})$ more generally indicates that in the basal plane and in (001) planes with small k_z values $\rho(\mathbf{p})$ may be described as a slice of the free-electron sphere modulated by the FS topology of Be. However, as one moves away from the zone center along the (001) direction and FS crossings disappear, the ''occupied region'' (i.e., region of high momentum density) in Be roughly resembles the shape of the second BZ. (For useful depictions of the second BZ of Be see Fig. 4 of

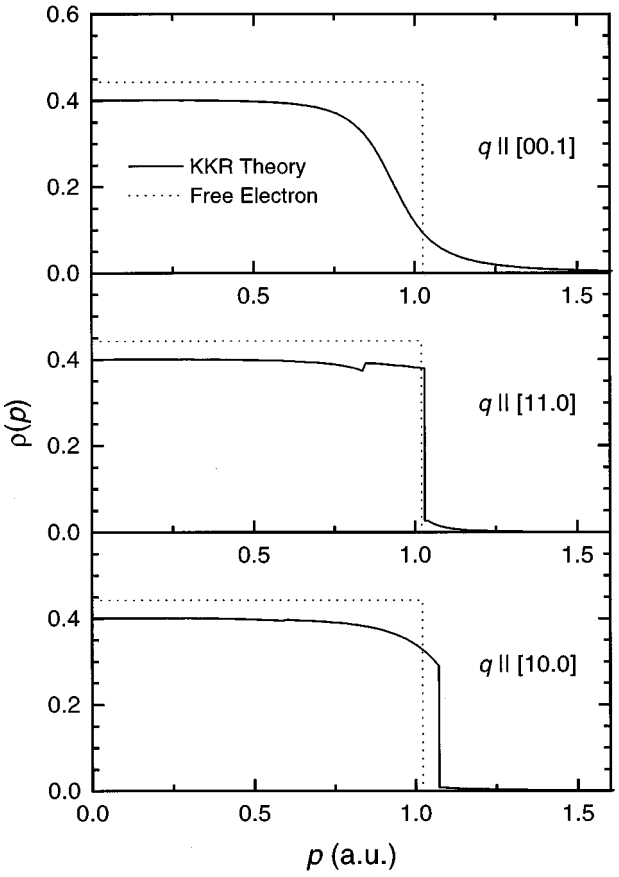

FIG. 4. Computed 3D momentum density along the three principal symmetry directions in Be. The corresponding free-electron results are shown for comparison (dotted).

Ref. 10, and also Fig. 4 of Ref. 12.) These remarks help explain some of the differences in the shapes of J_{001} and J_{110} in Fig. 3. For example, J_{001} decreases relatively rapidly near $p_z=0$ because here we are essentially intersecting the free-electron distribution. (The small rise in J_{001} near $p_z=0$ is a subtle FS effect.) On the other hand, J_{110} is quite flat for small momentum values since in this case we are integrating $\rho(\mathbf{p})$ in a vertical plane where the occupied area is little changed until one reaches the K point in the corner of the second BZ.

In a recent high-resolution Compton study of Li (see Fig. 1 of Ref. 28), the measured CP's along the three principal directions were found to be lower than the corresponding band theory computations at low momentum transfers. Interestingly, Fig. 3 does not show such a discrepancy between theory and experiment. This result could, however, be an artifact since our measurements extend only up to about 1.5 a.u. whereas the core contribution extends to much higher momenta. In order to establish this point more clearly, Compton data for higher momentum transfers in Be will be valuable. Then the core contribution could be separated from the total CP, allowing a more satisfactory comparison between theory and experiment at low momenta where the shape of the CP is dominated by the valence electrons.

Figure 5 considers the anisotropy $\Delta J=J_{001}-J_{110}$, and provides further insight into the behavior of CP's. In this way, as the isotropic parts of the profiles are removed, one is

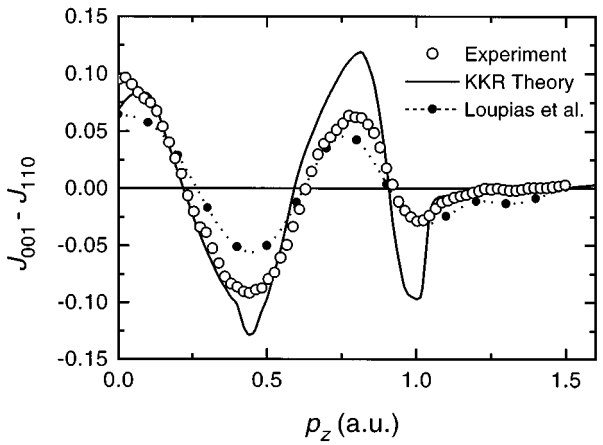

FIG. 5. Experimental anisotropy profile, $J_{001}-J_{110}$, is shown in comparison with the earlier 0.1 a.u. resolution Compton data of Loupias *et al.* (Ref. 1), and the present calculations. The size of the plotting symbol corresponds to statistical error.

better able to focus on the structure in the CP's. The shape of ΔJ is thus insensitive to the details of a number of uncertainties inherent in comparing theory and experiment; notable among these are (i) data analysis, in particular, background subtraction and absorption correction discussed in Sec. II above; (ii) the contribution from the $1s$ core which is isotropic even though it appears to be asymmetric[16] in Be as a function of momentum transfer; (iii) multiple scattering contribution which also does not possess any noticeable directional dependence. However, even an isotropic contribution can influence the amplitude of ΔJ indirectly via the normalization of the profile.

Figure 5 shows that the characteristic oscillations of the measured ΔJ curve are reproduced quite well by the theory, including the asymmetric shape of the peak at about 0.8 a.u., and the dip around 0.4 a.u. Since all profiles are normalized similarly, the area under ΔJ is zero, and ΔJ is expected to possess an oscillatory behavior. The amplitudes of the theoretical and experimental curves in Fig. 5 are similar for extrema around $p_z=0$ and $p_z=0.4$ a.u. Notably, around $p_z=0$, theory predicts a small decrease while the experiment shows an increase; this effect arises from a dip at $p_z=0$ in the computed [00.1] CP, which is present also in the computations of Ref. 11. The theoretical anisotropy is, however, more pronounced for extrema around $p_z=0.8$ a.u. and 1.0 a.u. and may reflect electron correlation effects, a point to which we return below. Incidentally, our data are consistent with the lower-resolution earlier Compton data of Loupias *et al.*[1]

It is necessary to take derivatives of the CP's in order to enhance and identify Fermi surface related structure in the data. Straight numerical differentiation is not sensible since with our statistics the high frequency noise becomes unacceptable. Smoothing of the data by averaging over multiple bins is also not appropriate as it would lead to a loss of resolution. We have empirically settled down to take derivatives via Fourier transform with simultaneous low-pass filtering. We have used a cosine shaped filter where the cutoff frequency corresponds to 0.04 a.u.

Figure 6 considers the first derivatives of the CP's. The unbroadened theory curves (dotted) display a number of FS features marked by various letters. A detailed analysis shows

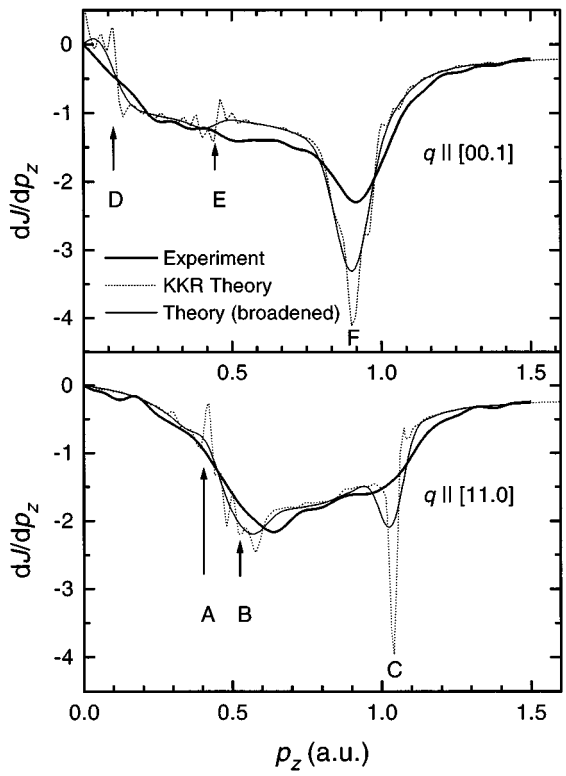

FIG. 6. First derivatives of the experimental and theoretical Compton profiles along the [00.1] and [11.0] directions. The theoretical derivatives without resolution broadening (dotted lines) are also shown in order to more clearly expose various Fermi surface features in the spectra, denoted by letters A–F, discussed in the text.

that along [11.0], the structure A at ≈ 0.4 a.u. arises from cigar sheets, the broad feature B around 0.55 a.u. from a combination of coronets and cigars, while the sharp dip C at about 1 a.u. is due to the surface of the cigar in the third BZ around the K point in the basal plane. Along [00.1], D and E at about 0.1 a.u. and 0.5 a.u., respectively, mark the vertical dimensions of the coronets and the cigar; the prominent dip F is not a FS feature but is related to the position of the top surface of the second BZ along [00.1], where, as we pointed out in connection with Fig. 4 above, the momentum density decreases rapidly.

Important for the present comparison between theory and experiment in Fig. 6 are the smoothed theoretical derivative spectra (thin solid); these curves include the effect of experimental resolution broadening in the computation, and have been processed in a manner identical to that used in obtaining the smoothed experimental derivatives (thick solid) via a low-pass filter as indicated before in the text. By comparing the dotted and thin solid curves, we see that the broadening and filtering process essentially washes out all features in the theoretical spectra except F and C. It is clear, therefore, that the combination of resolution and statistics employed in this experiment is not adequate for observing features A, B, D, and E.

Turning to features F and C, F is observed clearly in the experimental [00.1] CP, but the width of F in the experimental curve is larger than theory. On the other hand, no clear dip corresponding to C in the [11.0] data is discernible.[29] This may indicate that C suffers a rather large intrinsic broadening in the actual system. Note that since C arises from electron pockets of fairly small cross section in the basal plane, C may be rather sensitive to the crystal orientation. In any event, high-resolution, high statistics Compton measurements on Be and other relatively simple systems should give insight into these questions, in addition to allowing the possibility of observing the aforementioned FS signatures A, B, D, and E. In Be, it will be best to measure the Compton profile along a direction in the basal plane where the FS cutoff is sharp and unencumbered by the presence of nearby gaps or other delicate band structure features (with reference to Fig. 4, bottom panel, [10.0] direction appears to be a good candidate).

Figures 3, 5, and 6 all show that the features at 0.9 a.u. in the (001) and 1 a.u. in the (110) spectrum are clearly narrower in the theory compared to the experiment. In a recent high-resolution Compton study of Li, Sakurai *et al.*[28] report a similar smearing of the FS features, and suggest that this discrepancy originates from electron correlation effects beyond the LDA approximated in the standard band theory based treatment of the CP's. Other mechanisms that may play a role in this regard are the breakdown of the impulse approximation especially for relatively low recoil energies,[30] and possible electron-phonon effects. Further work to pin down the origin of this discrepancy should prove most interesting.

V. SUMMARY AND CONCLUSIONS

In summary, we have reported high-resolution Compton scattering measurements in Be together with corresponding highly accurate first-principles all-electron computations within the band theory framework. These are results of experiments carried out on the newly developed crystal spectrometer at the Brookhaven light source which is capable of a record momentum resolution [full width at half maximum (FWHM)] of 0.02 a.u. Compton profiles from two single crystals with surface normals along the [00.1] and [11.0] directions are presented and discussed. The overall shapes of the experimental directional profiles J_{001} and J_{110}, the anisotropy $J_{001}-J_{110}$, as well as the first derivatives of the spectra are in reasonable accord with the theoretical predictions. More important in connection with fermiology related issues, however, is the fine structure in the data, and in this regard there are significant discrepancies between the theory and experiment. In particular, several features in the observed spectra are substantially broader than the computations, reflecting presumably the effects of electron correlations beyond the local density approximation (LDA), and possibly also the breakdown of the impulse approximation, and other mechanisms. Further, a theoretically predicted feature associated with the cigar Fermi surface sheet is not observed in the measured spectra. We comment on these points, and suggest that a higher statistics Compton study of Be will be valuable. The present work clearly demonstrates that the high-resolution Compton technique constitutes a useful tool for investigating fermiology related issues in materials.

ACKNOWLEDGMENTS

It is a pleasure to acknowledge F. Sette for lending us his crystal bender, J. Schneider for the Be samples, and J. Felsteiner for his multiple scattering calculation. This work is supported by the U.S. Department of Energy under Contract Nos. DE-AC02-76CH00016 and W-31-109-ENG-38, including a subcontract to Northeastern University, and the Academy of Finland (Contract No. 8582), and benefited from the allocation of supercomputer time at the NERSC and Pittsburgh Supercomputer centers.

APPENDIX

The exact formula for the partial derivative relative to the scattering angle θ is

$$\frac{\partial p_z}{\partial \theta} = \frac{mc\omega_1\omega_2[\omega_1^2+\omega_2^2-\omega_1\omega_2+mc^2(\omega_1-\omega_2)-\omega_1\omega_2\cos\theta]\sin\theta}{mc^2(\omega_1^2+\omega_2^2-2\omega_1\omega_2\cos\theta)^{3/2}}. \tag{A1}$$

At the limit $\omega_1 \approx \omega_2$ this leads to the approximative formula (2) in Ref. 25 which is not valid in our case.

*Permanent address: Academy of Mining and Metallurgy, Cracow, Al. Mickiewicza 30, Poland.

[1] G. Loupias, J. Petiau, A. Issolah, and M. Schneider, Phys. Status Solidi B **102**, 79 (1980).

[2] Y. Sakurai, M. Ito, T. Urai, Y. Tanaka, N. Sakai, T. Iwazumi, H. Kawata, M. Ando, and N. Shiotani, Rev. Sci. Instrum. **63**, 1190 (1992).

[3] A. Berthold, S. Mourikis, J.R. Schmitz, W. Schülke, and H. Schulte-Schrepping, Nucl. Instrum. Methods A **317**, 373 (1992).

[4] V. Stojanoff, K. Hämäläinen, D.P. Siddons, L.E. Berman, J.B. Hastings, S. Cramer, and G. Smith, Rev. Sci. Instrum. **63**, 1125 (1992).

[5] C.-C. Kao, K. Hämäläinen, M. Krisch, D.P. Siddons, J.B. Hastings, and T. Oversluizen, Rev. Sci. Instrum. **66**, 1699 (1995).

[6] W. Schülke and H. Nagasawa, Nucl. Instrum. Methods **222**, 203 (1984).

[7] J.B. Brown, Philos. Mag. B **26**, 1377 (1972).

[8] F.K. Larsen, M.S. Lehmann, and M. Merisalo, Acta Crystallogr., Sec. A **36**, 159 (1980).

[9] S. Manninen and P. Suortti, Philos. Mag. B **40**, 199 (1979).

[10] R. Currat, P.D. DeCicco, and R. Kaplow, Phys. Rev. B **3**, 243 (1971).

[11] M.Y. Chou, P.K. Lam, M.L. Cohen, G. Loupias, J. Chomilier, and J. Petiau, Phys. Rev. Lett. **49**, 1452 (1982); M.Y. Chou, P.K. Lam, and Marvin L. Cohen, Phys. Rev. B **28**, 1696 (1983).

[12] N.K. Hansen, P. Pattison, and J.R. Schneider, Z. Phys. B **35**, 215 (1979).

[13] A.T. Stewart, J.B. Shand, J.J. Donaghy, and J.H. Kusmiss, Phys. Rev. **128**, 118 (1962).

[14] R. Dovesi, C. Pisani, F. Ricca, and C. Roetti, Phys. Rev. B **25**, 3731 (1982).

[15] P. Platzman and N. Tzoar, Phys. Rev. A **139**, 410 (1965).

[16] A. Issolah, Y. Garreau, B. Levy, and G. Loupias, Phys. Rev. B **44**, 11 029 (1991).

[17] The analyzer crystal assembly was designed by Dr. F. Sette (ESRF).

[18] P. Holm, Phys. Rev. A **37**, 3706 (1988).

[19] J. Felsteiner (private communication).

[20] F. Bell and J. Felsteiner, Nucl. Instrum. Methods B **101**, 379 (1995).

[21] A. Bansil and S. Kaprzyk, Phys. Rev. B **43**, 10 335 (1991); S. Kaprzyk and A. Bansil, *ibid.* **42**, 7358 (1990); A. Bansil, S. Kaprzyk, and J. Toboła, in *Application of Multiple Scattering Theory to Materials Science*, edited by W. H. Butler *et al.*, MRS Symposia Proceedings No. 253 (Materials Research Society, Pittsburgh, 1992), p. 505.

[22] U. von Barth and L. Hedin, J. Phys. C **5**, 1629 (1972).

[23] G. Lehmann and M. Taut, Phys. Status Solidi B **54**, 469 (1972).

[24] L. Lam and P.M. Platzman, Phys. Rev. B **9,** 5122 (1974).

[25] N. Shiotani, N. Sakai, F. Itoh, M. Sakurai, H. Kawata, Y. Amemiya, and M. Ando, Nucl. Instrum. Methods, A **275**, 447 (1989).

[26] T.H. Loucks and P.H. Cutler, Phys. Rev. **133**, A819 (1964).

[27] The theoretical and experimental CP's are not listed in a tabular form in the interest of brevity, but may be obtained from the authors upon request.

[28] Y. Sakurai, Y. Tanaka, A. Bansil, S. Kaprzyk, A.T. Stewart, Y. Nagashima, T. Hyodo, S. Nanao, H. Kawata, and N. Shiotani, Phys. Rev. Lett. **74**, 2252 (1995).

[29] Notably, preliminary results presented at the 2nd International Compton Scattering and Fermiology meeting (Tokyo, August 28–31, 1995) by N. Shiotani, Y. Ito, and collaborators hint at the existence of a dip corresponding to the structure *C* in their [11.0] Be data.

[30] W. Schülke (unpublished).